Articles in PresS. Am J Physiol Heart Circ Physiol (December 21, 2007). doi:10.1152/ajpheart.00816.2007

# Microtopography and Flow Modulate the Direction of Endothelial Cell Migration

P. Uttayarat[1], M. Chen[1], M. Li[2], F. D. Allen[2], R. J. Composto[1] and P. I. Lelkes[2]

[1] Department of Materials Science and Engineering, University of Pennsylvania, Philadelphia, PA 19104

[2] School of Biomedical Engineering, Science and Health Systems, Drexel University, Philadelphia, PA 19104

Correspondence:

Dr. Peter I. Lelkes

School of Biomedical Engineering, Science and Health Systems, Drexel University

Philadelphia, PA 19104

pilelkes@drexel.edu

215.762.2071

**Running head**: endothelial cell migration: microgrooves vs. flow

**ABSTRACT**

The migration of vascular endothelial cells under flow can be modulated by the addition of chemical or mechanical stimuli. The aim of this study was to investigate how topographic cues derived from a substrate containing three-dimensional (3-D) microtopography interact with fluid shear stress in directing endothelial cell migration. Subconfluent bovine aortic endothelial cells were seeded on fibronectin-coated poly(dimethylsiloxane) (PDMS) substrates patterned with a combinatorial array of parallel and orthogonal microgrooves ranging from 2 to 5 μm in width at a constant depth of 1 μm. During 4 h time-lapse observation in the absence of flow, the majority of the pre-aligned cells migrated parallel to the grooves with the distribution of their focal adhesions (FAs) depending on the groove width. No change in this migratory pattern was observed after the cells were exposed to moderate shear stress (13.5 dyn/cm$^2$), irrespective of groove direction with respect to flow. After 4 h exposure to high shear stress (58 dyn/cm$^2$) parallel to the grooves, the cells continued to migrate in the direction of both grooves and flow. By contrast, when microgrooves were oriented perpendicular to flow, most cells migrated orthogonal to the grooves and downstream with flow. Despite the change in the cells' migration direction under high shear stress, most FAs and actin microfilaments maintained their original alignment parallel to the grooves, suggesting that topographic cues were more effective than those derived from shear stress in guiding the orientation of cytoskeletal and adhesion proteins during the initial exposure to flow.

**Key words:** endothelial cell alignment, endothelial cell migration, microgrooves, shear stress, focal adhesion

## INTRODUCTION

Endothelial cell (EC) migration plays a critical role in vascular remodeling processes such as angiogenesis, vasculogenesis and wound healing (24, 25, 27, 30, 35). The fluid shear stress experienced by vascular endothelial cells in the *in vivo* hemodynamic milieu provides an important mechanical cue that can direct cell migration and induce the activation of biochemical processes (8, 15, 35). Integrins (16, 38), focal adhesion (FA) proteins (24, 26, 27, 37) cytoskeletal components (6, 16, 18, 19, 23, 27, 28, 34, 37), regulatory proteins (13, 35, 41) and intracellular ion concentrations (12, 28) are amongst the molecular components that regulate the morphological changes and the physiological responses of endothelial cell migration upon exposure to shear stress. Therefore, the modulation of EC migration in such vascular remodeling processes requires an understanding of how the cells interact and respond to the shear stress environment.

In physical terms, cell migration proceeds in three coordinated steps: a) membrane extension and formation of FAs at the leading edge, b) forward movement of the cell body through contraction of the actin cytoskeleton by myosin-based motors and c) detachment of the cell's trailing edge which completes the cycle of the migration process (25, 30, 35). When cultured cells are exposed to a steady, laminar flow, lamellipodial protrusions develop within minutes from the cell periphery in the direction of flow (27, 29), followed by the recruitment of focal adhesion kinase (FAK) at focal adhesion sites underneath the newly formed lamellipodia (27). Shear stress also polarizes FAs to localize at the leading edge and the trailing edge of the cell before its persistent migration downstream with the flow (27). In addition to the alignment of cell shape, both

actin microfilaments and microtubules remodel and align in the direction of flow (16, 18, 28). Thus, the integrated system of FAs and cytoskeleton is essential in mediating the physical process of cell migration.

Directional EC migration *in vitro* can be induced by chemical stimuli, either soluble in the medium (chemotaxis) (1, 10, 11, 14) or immobilized on the substrate surface (haptotaxis) (22, 24), as well as by mechanical stimuli (mechanotaxis), such as fluid shear stress (24, 27, 35). The increase in shear stress magnitude from 5 to 45 dyn/cm$^2$ enhances the migration distance of human umbilical vein ECs about two-fold into the denuded area after 24 h exposure to flow (38). With the combination of both haptotactic and mechanotactic cues arranged orthogonally to each other, these two stimuli competitively direct EC migration (24). The increase in shear stress from 2 to 10 dyn/cm$^2$ is shown to effectively switch the direction of about 50% of ECs to migrate with the flow across the haptotactically-derived collagen tracks over a 16 h period (24). This result suggests that above a certain threshold, fluid shear stress can significantly modulate cell migration on adhesive substrata.

In this study, we examined the migration of subconfluent bovine aortic endothelial cells (BAECs) on PDMS substrates patterned with a combinatorial array of 3-D microgrooves under static (no shear) conditions and when exposed to two different levels of fluid shear stress. Based on our previous study (40) of BAEC alignment on the 3-D microgrooves, we hypothesized that the spatial localization of FAs along the groove depth would guide the directional cell migration. Results indicate that while the majority of cells migrated parallel to the grooves under static condition, the direction of cell migration under flow depended on the magnitude, as well as the direction of fluid shear

stress with respect to the orientation of microgrooves. This interplay between substrate microtopography and shear stress suggests that the direction of cell migration can be modulated by the spatial localization and the forced re-organization of FAs. For the development of vascular prostheses, these microgrooved surfaces can promote the endothelialization process in small caliber prosthetic grafts and facilitate the grafts' healing after bypass surgery.

## MATERIALS AND METHODS

*Microfabrication of the combinatorial array of microgrooves.* The combinatorial 4×8 array of microgrooves, containing four sets of groove patterns organized in the horizontal and vertical directions, was first fabricated on a silicon (Si) wafer (Fig. 1A) by electron-beam (e-beam) lithography and reactive ion etching (RIE) at the Microfabrication Laboratory, University of Pennsylvania. For the symmetric patterns, 5×5, 3×3 and 2×2, microgrooves contained ridges and channels of equal widths, whereas for the asymmetric 5×2 pattern, the widths of the ridges and channels were 5 and 2 μm, respectively. Each groove area, 500×500 $\mu m^2$, was separated by a distance of 500 μm.

For e-beam lithography, the pre-cleaned Si wafer (Silicon Quest International; Santa Clara, CA) (40) was spin-coated with poly(methyl methacrylate) (PMMA) (MicroChem Corp, Newton, MA) at 3000 rpm for 45 s to obtain a 400-nm resist layer. The PMMA coated wafer was then baked at 110°C for 10 min before irradiation with e-beam. The microgroove patterns were designed and generated using commercially available software (Raith, Ronkonkoma, NY). E-beam lithography was performed on a JEOL (JSM-6400, Peabody; MA) scanning electron microscope at 15 mm working

distance, 50x magnification, 10 nA e-beam current, and 400 μC/cm$^2$ area dose. Following e-beam writing, the resist was developed for 45 s in a solution of 1:3 (v/v) methyl isobutyl ketone/isopropanol, followed by rinsing in isopropanol for 45 s. After the evaporation of Nichrome IV to serve as a photomask (40), the wafer was then dry etched by RIE to create groove depth of 1 μm. This depth dimension was chosen based on our previous study of BAEC alignment (40). The finished Si wafer served as a mold to replicate the combinatorial array of microgrooves on the PDMS substrates.

*Preparation and Characterization of PDMS substrates.* All PDMS substrates were prepared from Sylgard 184 Silicone Elastomer kit (Robert McKeown Company, Branchburg, NJ) and sterilized as previously described (40). The microgroove profiles on the PDMS replicas were inspected by scanning electron microscopy, FEI Strata DB235 Focused Ion Beam (FEI, Hillsboro, OR), at an acceleration voltage of 10 keV. To observe cell migration in real-time, the PDMS substrates were cut into circles (2 cm diameter) for static experiments, and rectangles (2.5 cm wide × 6.0 cm long × 0.1 cm thick) for experiments conducted under flow. After sterilization, all substrates were incubated in a 10 μg/ml fibronectin (Fn) solution for 15 h. The non-specific adhesion was blocked with 1% BSA (Fraction V; Sigma) (40). As we have previously demonstrated (39, 40), this extended incubation period in the Fn solution produced a uniform coverage of Fn coating on both grooved and smooth surfaces.

*Assembly of the flow system.* The parallel plate flow chamber device (21), with sealed glass windows on both the upper and the lower plates, was custom-built from polysulfone (McMaster-Carr, Dayton, NJ) at the Research Instrumentation Shop, University of

Pennsylvania. A Teflon gasket (McMaster-Carr) was inserted between the two plates, creating a rectangular flow channel (1.35 cm wide × 4.30 cm long × 0.025 cm high) for the circulation of medium. After each substrate was assembled on the lower plate, the two plates were screwed tight and connected to the flow loop, which consisted of a peristaltic pump (Cole Palmer, Vernon Hills, IL), two pulse dampeners to generate a steady, laminar flow (17), a parallel plate flow chamber and a medium reservoir (16, 17, 24, 36). The medium was maintained at 37°C throughout the entire experiment outside the incubator by keeping the reservoir and the pulse dampeners in temperature-controlled water baths.

*Cell culture.* Bovine aortic endothelial cells *(*BAECs) were isolated and cultured in gelatin-coated T75 flasks using complete DMEM (Mediatech) supplemented with 10% FBS (Hyclone), 1 mg/ml glucose, 0.3 mg/ml L-glutamine, 10 μg/ml streptomycin, 10 U/ml penicillin, and 25 ng/ml amphotericin at 37°C in 95% air/5% $CO_2$ as previously described (40). Cells were sub-cultured every two days and used at passages 8-12.

*Cell labeling with fluorescent tracker.* For real-time fluorescence visualization, BAECs were pre-labeled with 1,1'- dioctadecyl-3,3,3',3'-tetramethylindocarbocynanine perchlorate (DiI) (Molecular Probes) in suspension in serum-free DMEM according to the manufacturer's instructions. In brief, the cell suspension was first diluted to about 500,000 cells per 1 ml of serum-free DMEM containing a 1:100 (v/v) solution of DiI and incubated for 15 min at 37°C. The cells were then pelleted by centrifugation at 400 rpm for 4 min at 25°C, washed twice, and finally re-suspended in serum-free DMEM. The uniform DiI labeling was confirmed by flow cytometry and fluorescence imaging (data not shown).

*Time-lapse observation of individual BAEC migration***.** The DiI-labeled cells were seeded on the PDMS substrates at a density of 5,000 cells/cm$^2$ (about 100,000 – 150,000 cells in total) in serum-free DMEM to reduce the interference of serum proteins with the pre-coated Fn on the PDMS substrates. Cells were allowed to attach and spread for 2 h inside the incubator. Before the start of all time-lapse recording on the microscope outside the incubator, cells were refreshed in DMEM without bicarbonate, supplemented with 25mM HEPES (Cellgro) to maintain a physiological pH in the absence of $CO_2$, 2 μg/ml ascorbic acid (Sigma) as an antioxidant to minimize bleaching of DiI, and 0.5% FBS.

For the static experiment, circular PDMS substrates, pre-seeded with BAECs as described above, were placed inside a 12-well tissue culture plate. A heat pad underneath the well plate provided a constant temperature of 37°C. To record cell migration under flow, the pre-seeded PDMS substrates were placed inside the parallel plate flow chamber and assembled onto the microscope stage (Nikon TE 2000U equipped with a Prior ProScan II motorized stage). A steady, laminar shear stress of 13.5 or 58 dyn/cm$^2$ was applied for the entire 4 h duration of the experiments. These two magnitudes of shear stress were chosen based on previous studies (24, 31, 38). The corresponding Reynolds numbers for the two shear stress levels are 25 and 106, respectively.

Phase contrast images of selected cells, about 10-20, on each microgroove pattern within a given row (four parallel and four perpendicular to the flow, see Fig. 1A) were first captured using the Northern Eclipse software (P3I, Glen Mills, PA) to specify the initial locations of these cells. The motorized stage then moved accordingly to the specified locations on all eight patterns while the time-lapse fluorescence images were acquired with a 10x objective lens every 15 min for 4 h. Cell viability was assessed with

the Live-Dead assay (Molecular Probes) at the termination of each experiment. Viability remained at > 95% for all experiments.

*Scratch wound assay.* Similar to the effect of cholesterol that slows down cell migration (17), we consider that the DiI accumulation in the lipid bilayer of the cell membrane might cause a decrease in BAEC migration velocity. The effect of DiI on EC migration was evaluated by a scratch wound assay. Non-labeled and DiI-labeled BAECs were seeded at a density of 130,000-150,000 cells/cm$^2$ onto 6-well tissue culture plates, which had been pre-coated with 10 μg/ml Fn. This cell density was chosen such that a confluent monolayer was reached within 16 h to minimize DiI dilution after cell division. Multiple strips within the same well were scratched using a 200-μL pipette tip (17). Detached cells were washed away with PBS, followed by the addition of fresh DMEM without bicarbonate supplemented with 25 mM HEPES and 0.5 % FBS. The temperature was maintained at 37°C by the heat pad underneath the well plate. Time-lapse phase contrast images of cells migrating away from the wound edge were acquired with a 4x objective lens every 15 min for 4 h. Approximately 8 distances between the two wound edges on each image were measured at 1, 2, 3, and 4 h, respectively. The migration velocity was calculated by dividing the total distance each wound edge had migrated by the set time points. The migration velocity of DiI-labeled BAECs was slower by 29 ± 3.4 % ($p$ < 0.05, n = 4) than that of unstained BAECs. This decrease in cell migration velocity remained constant throughout the entire duration of 4 h after wounding.

*Fluorescent visualization of focal adhesions and actin microfilaments.* Actin microfilaments and FAs were visualized by fluorescent staining and indirect immunostaining, respectively, as previously described (40) at the termination of the migration experiments. In brief, BAECs without DiI labeling were fixed in 4% formaldehyde (Electron Microscopy Sciences, Hatfield, PA) for 20 min at room temperature. Cells were then permeabilized in 0.5% Triton X-100 for 5 min, washed twice with PBS, and blocked with 1% BSA solution for 30 min. To stain for FAs, we used a mouse monoclonal anti-vinculin IgG (1:200; Chemicon) as a primary antibody and Alexa Fluor 488-conjugated chicken anti-mouse IgG (1:1000; Molecular Probes) as a secondary antibody. The primary and secondary staining steps took 1 h and 45 min, respectively, at room temperature, with three washes in PBS after each staining step. To visualize actin microfilaments, cells were further incubated with TRITC-conjugated phalloidin (1:1000; Sigma) for 45 min at room temperature. After the last wash in PBS, the samples were mounted on microscope glass slides and a 20-µl drop of ProLong Gold (Molecular Probes) was added before covering with glass cover slips. The samples were then examined by conventional (Leica DMRX) and confocal (Nikon Eclipse TE-300 equipped with BioRad Radiance 2000-MP) fluorescence microscopy. For confocal microscopy, the confocal image was prepared by overlaying a stack of images taken at a step size of 0.2 µm over a distance of about 8 µm from the floor of the channels upto the apical surface of the cells.

*Data analysis***.** Cell orientation on microgrooves was characterized as previously described (40). Briefly, cells were defined as “aligned” if they exhibited an elongated

shape and their major axes were within 20° with respect to the grooves. Elongated cells with their major axes oriented between 20° to 90° to the grooves were defined as "non-aligned". Cells were described as "isotropic" if they spread uniformly, or randomly extended cell processes equidistant from the center of the cell body.

Cell migration was traced by the movement of cell nuclei using the tracking function in Image-Pro Plus software (version 5.0, P3I, Glen Mills, PA). The directions of cell migration were categorized as parallel, transverse, randomly oscillating, or mixed, with respect to the grooves. BAECs that migrated parallel to or across several ridges and channels were grouped into the parallel and transverse directions, respectively, whereas cells that randomly migrated in several directions but ended up near their original locations were defined as randomly oscillating. The term "mixed" describes cells that exhibited a mixture of parallel, transverse or randomly oscillating migration. The velocity of cell migration was calculated from the traced total distance over the experimental time of 4 h.

Changes in cell shape due to flow were quantified by calculating the shape factor of individual cells. The shape factor is defined as the ratio $4\pi A/P^2$, where $A$ and $P$ are the cell area and cell perimeter, respectively. The shape factor approaches 0 as the cells assume a highly elongated shape and 1 as the cells fully spread and assume a more rounded geometry. After the termination of cell migration experiments, the shape factor was determined using TRITC-conjugated phalloidin to delineate cell boundaries and Northern Eclipse software to calculate cell area, cell perimeter and shape factor.

*Statistics*. All values are expressed as mean ± standard error (SE). For cell orientation, data were collected from 3 independent experiments, each with 2 replicates. Approximately 200 cells were analyzed for their orientation on each of the microgroove patterns. For cell migration, data were collected from 5-7 independent experiments for each of the static and flow conditions. To calculate shape factor, data were collected for static and high shear conditions, each from 3 independent experiments with a total of approximately 80 to 110 cells. Statistical analysis was performed by one-way ANOVA, followed by the *post hoc* Tukey's test with $p \leq 0.05$ being statistically significance.

**RESULTS**

*Characterization of microgroove patterns.* The dimensions of all four microgroove patterns were characterized by SEM (Figs. 1B to 1E) and are tabulated in Table 1. The average depth dimension of microgrooves was 1.2 ± 0.02 μm. Due to the surface tension of the base elastomer, the mixture did not totally wet the channels before it was cross-linked, resulting in channels that tapered slightly by 27.0 ± 1.9° from a perfect vertical step. To account for this, the symmetry and the dimensions of microgrooves were determined by measuring the widths of the ridges and channels at the position half way down the groove depth.

*Endothelial cells elongate and align in the direction of grooves.* In agreement with our previous data (40), the vast majority of BAECs, 92.1 ± 1.0 %, aligned within 20° parallel to the grooves, independent of the groove width within 1 h of attachment (Fig. 2). In this

aligned population, 56.7 ± 2.8 % of the cells had their major axes formed within 5° with respect to the groove direction. About 8.4 ± 0.9 % of the total cells remained non-aligned or isotropic. These data demonstrate that the microgrooved substrate induces the rapid initial BAEC elongation and alignment prior to the onset of time-lapse measurements of cell migration.

*Microgrooves guide the direction of cell migration in the absence of flow.* The direction of BAEC migration on the microgrooved PDMS substrates was classified as belonging to one of the four distinctive groups: parallel, transverse, randomly oscillating and mixed. The direction and the velocity of BAEC migration on microgrooves are presented as a function of groove width in Figs. 3A and 3B, respectively. A majority of BAECs, 54.5 ± 3.9 %, migrated parallel to the grooves (Fig. 3A), independent of the groove width on the symmetric patterns, whereas there was a slight decrease ($p > 0.05$) to 43.6 ± 4.4 % on the asymmetric 5×2 pattern. As the groove width decreased from 5 to 2 μm, more cells were able to migrate across the channels, with a maximum found on the 5×2 pattern where 16.0 ± 3.6 % of the cells ($p < 0.05$) migrated transverse to the grooves. Thus, the directional cell migration on microgrooves can be modulated by fine tuning the groove dimension at the micron scale. This increase in BAEC migration transverse to the grooves on the 5×2 pattern with the decrease in cell migration in the parallel direction suggests that the directional control also depends to some extent on the inherent symmetry of the pattern.

The migration velocity of BAECs (Fig. 3B) parallel to the grooves was similar on all microgroove patterns ($p > 0.05$) and statistically not different from that on smooth

surfaces, where the cells' migration velocity was 19.9 ± 1.5 μm/h. This latter value is in good agreement with the reported migration velocity (35) of endothelial cells on a glass substrate coated with a similar Fn surface density. Averaged across all the patterns, the cell migration velocities in the parallel and the transverse directions were 19.0 ± 1.0 and 15.4 ± 1.6 μm/h ($p > 0.05$), respectively. In our system, the migration velocity in the parallel direction was significantly higher ($p < 0.05$) than the transverse direction only on the 3×3 and the 2×2 patterns. In addition, the rate of cell migration (migration distance/30 min interval) remained constant (data not shown) in both parallel and transverse directions over the duration of 4 h, in agreement with the constant cell migration rate on Fn-coated glass slides (27). This finding assured us that the cell migration velocity was steady throughout the experimental time, allowing the comparison of our data to previous studies, both longer term, i.e., 24 h (3, 4, 7, 16-18, 24, 28, 38, 41), and shorter term, e.g. 2 h (27, 35).

*Fluid shear stress can add to or compete with microgrooves in guiding the direction of endothelial cell migration*. Depending on the groove orientation with respect to the flow, fluid shear stress can add to or compete with microgroove-derived cues in directing BAEC migration. When flow was applied parallel to microgrooves (Fig. 4A), shear stress enhanced BAEC migration parallel to the grooves. At the high shear stress level (58 dyn/cm$^2$), 89.0 ± 2.5 % of BAECs migrated in the direction of both grooves and flow on all four microgroove patterns, significantly higher ($p < 0.05$) than the moderate shear stress (13.5 dyn/cm$^2$) and static conditions. By contrast, during our observation time of 4 h, only 4.3 ± 0.5 % of BAECs migrated in a straight line with the flow at high shear stress

on a smooth surface. As seen in Fig. 4A (top images), upon entering the 3×3 pattern under flow, a cell (solid arrows) immediately migrated parallel to the grooves, while another cell (arrow heads) on the same area preferentially extended filopodium from the leading edge of the cell along the channels. This result demonstrates that microgrooves can potently accentuate directional cell migration parallel to the flow. There was also a trend of a slight increase in cell migration velocity with increasing magnitude of shear stress from 19.6 ± 1.4 μm/h at moderate shear to 24.3 ± 1.0 μm/h at high shear.

At moderate shear stress, about 5.9 ± 1.1 % of the individual, non-dividing BAECs migrated upstream against the flow direction. For cells dividing under moderate shear stress, two daughter cells separated and then migrated in their respective downstream and upstream directions, whereas at high shear stress, the daughter cell that first migrated upstream against the flow eventually changed its direction to migrate downstream with the flow. We conclude that cell migration parallel to the grooves is much more sensitive to the magnitude of the applied fluid shear stress than the variation in groove widths (2-5 μm) or the groove symmetry.

When flow was applied perpendicular to microgrooves, cues derived from shear stress competed with those from the topography of the microgrooves in guiding BAEC migration. At high shear (Fig. 4B), 68.6 ± 1.50 % ($p < 0.05$) of BAECs migrated transverse to the grooves on all four patterns, independent of the groove width. Within our observation time of 4 h, moderate shear stress only minimally affected cell migration transverse to the microgrooves. Interestingly, at high shear, the cells migrated transverse to the grooves in two different manners (top images, 5×5 pattern, Fig. 4B). In approximately half of the observed events, cells extended protrusions from both ends of

the cell body (arrow heads) to the next downstream ridge and then moved forward in the downstream direction, which was orthogonal to the grooves. In the other half, the cells extended single protrusions from one end of the cell body, causing them to reorient away from the groove direction. The cells then continued their movement in this downstream direction with a cell body alignment at a 30.0 ± 1.1° angle (solid arrows) to the grooves. In addition, the cell migration velocity at high shear was 17.8 ± 1.0 μm/h, slightly greater ($p > 0.05$) than the velocity at moderate shear (14 ± 1.4 μm/h). Similar to the switch in the migration direction of endothelial cells on glass surfaces patterned with collagen gradients (24), a threshold level of shear stress is required to compete with the adhesive interaction between cells and their underlying microgrooved substrata. In our study, the shear stress threshold appears to be between 13.5 and 58 dyn/cm$^2$.

*Actin microfilaments align in the direction of grooves.* Under static condition (Fig. 5), most actin microfilaments formed a perimembrane web around the cell periphery, with a few bundles randomly stretched across the cells on the smooth surface (Fig. 5A), or aligned parallel to the grooves on the patterned surfaces (Figs. 5B and 5C). On the 5×5 and 5×2 patterns, the cell protrusions were also observed in the 5-μm (Fig. 5B) and the 2-μm (Fig. 5C) wide channels, in agreement with the real-time observation (top images, Fig. 4A) that the cells can extend filopodia inside the channels.

In response to high shear stress, the actin cytoskeleton remodeled to form extensive actin stress fibers on both smooth (Fig. 5D) and microgrooved (Fig. 5E and 5F) surfaces. Similar actin reorganization was also observed at moderate shear stress (data not shown). When the cells were attached to the microgrooved surfaces, the actin stress

fibers maintained their alignment parallel to the grooves regardless of flow direction (Figs. 5E and 5F). On the microgrooves oriented parallel to the flow (Fig. 5E), the channels provided tracks to guide the protrusions at the front of the cells (solid arrows) along and inside the channels, while those at the back (arrow heads) of the cells remained attached to the edge of the ridge. Orientation of the microgrooves perpendicular to the flow (Fig. 5F) resulted in the preferential termination of protrusions at the downstream side of the cell (solid arrows). Our data suggest that cues derived from fluid shear stress are important for actin remodeling, while the microtopographic cues provide a more effective guidance in orienting the alignment of these stress fibers within the 4 h period of exposure to flow.

*Localization of focal adhesions is groove-width dependent.* The distribution of FAs, as inferred from the localization of vinculin, was visualized by confocal microscopy. On smooth surfaces under static condition, FAs were concentrated at the cell periphery (Fig. 6A). Most FAs adopted an elongated shape of about 2.3 ± 0.2 μm in size, with the exception of a few highly elongated FAs (> 5 μm, solid arrow, Fig. 6A). On microgrooved surfaces, the localization of FAs depended on the dimension of groove width. For the 5×5 pattern with the widest groove width, FA distribution was almost equal inside the channels (42.2 ± 3.0 %, solid arrows, Fig. 6B) and on the ridges (46.7 ± 2.4%, arrow heads, Fig. 6B). A few FAs were observed to span along the groove sidewalls (open arrows, Fig. 6B). For narrower groove widths, fewer FAs (about 5.7 ± 1.3%) remained localized inside the channels as the majority of FAs formed along the groove sidewalls as well as on the ridges. On the 5×2 pattern, most FAs (78.2 ± 4.4 %,

arrow heads, Fig. 6C) formed on the ridge edges and aligned parallel to the grooves, similar to the 2×2 pattern (data not shown). These results indicate that when ECs are seeded on microgrooved surfaces in the absence of flow, the width of the groove is an important parameter that dictates the spatial distribution of FAs on the patterned substrate.

*Most focal adhesions align parallel to grooves*. Upon exposure to high shear, FAs became elongated and polarized towards the downstream and the upstream sides of the cells (Figs. 7A-7E). On smooth surfaces where BAECs had already aligned (Fig. 7A) or were in the process of re-aligning the major axes with the flow (Fig. 7B), most FAs could be found at the cell's edges. The alignment of FAs on microgrooved surfaces (Figs. 7C and 7D) was reminiscent of our observations of actin stress fibers on patterned surfaces with the majority of FAs maintaining their alignment parallel to the grooves regardless of groove orientation with respect to flow. For example, on the 3×3 pattern oriented parallel to the flow (Fig. 7C), most FAs formed along the ridge edge, with a long stretch of FA (solid arrow) spanning the groove sidewall before terminating on the ridge at the rear of the cell. Similarly, when the flow was applied perpendicular to the orientation of the grooves (5×2 pattern, Fig. 7D), most FAs formed along the ridge edge and aligned parallel to the grooves (dashed arrow), whereas a few FAs aligned in the direction of the flow (arrow heads). Interestingly, for this perpendicular orientation of grooves and flow (5×2 pattern, Fig. 7E), we also observed the formation of FAs in the flow direction underneath the cell protrusion on the downstream side of the cell (solid arrow) as the cell migrated across microgrooves. The remaining FAs around the cell periphery either re-

aligned their orientation (arrow head, Fig. 7E) with the flow or maintained their alignment (dashed arrow, Fig. 7E) with the grooves. This preferential alignment of both FAs and actin cytoskeleton with microgrooves may help strengthen cell retention during exposure to a high level of fluid shear stress.

*Subconfluent endothelial cells become flattened under flow*. In addition to visualizing the FA distribution, confocal microscopy allowed us to estimate the height of the cells by measuring the distance between the ridge plane and the cell's apical surface. The average height of subconfluent endothelial cells after exposure to high shear stress for 4 h was 1.4 ± 0.1 μm, compared to an average cell height of 2.5 ± 0.11 μm, in the absence of flow. This reduction in the cell height is in agreement with the atomic force microscopy (AFM) data (4) that the cell height decreased by about 50% in endothelial monolayers exposed to a shear stress of 12 dyn/cm$^2$ for 24 h.

*Flow induced endothelial cell spreading in the flow direction***.** As inferred from the shape factor, the 4 h exposure to flow induced cell spreading in the direction of flow on all smooth and microgrooved surfaces (Table 2). On microgrooves oriented parallel to flow, there was a trend of increasing shape factor at high shear stress compared to static conditions irrespective of groove widths. On microgrooves oriented perpendicular to flow, the same high shear stress significantly ($p < 0.05$) induced the extension of cell membrane downstream with the flow, resulting in about 38% increase in the cells' shape factor compared to static condition. This increase in shape factor of the cells that were initially aligned perpendicular to flow suggests that the flow-induced downstream

extension of cell membrane can gradually guide a cell through the process of re-aligning its major axis with flow.

## DISCUSSION

In this study we demonstrate that a 3-D microgroove topography provides a significant stimulus to mediate the directional migration of endothelial cells without confining individual cells to a single ridge or inside a channel. In the absence of fluid shear stress, our microgrooved substrate induces the spatial localization of FAs along the groove depth and the alignment of actin microfilaments parallel to the grooves. On the substrate with the widest channel (5 μm ridge × 5 μm channel), the equal distribution of FAs inside the channels as well as on top of the ridges directs the majority of cells to migrate parallel rather than perpendicular to the grooves. On the narrower channels (3×3, 2×2 and 5×2 patterns), most FAs localize and align on the ridge edge, thus allowing the cells to migrate both parallel and transverse to the grooves. The spatial localization of FAs over the 3-D microgrooves is a unique feature of our substrate that guides the directional endothelial cell migration and differs significantly from endothelial haptotaxis along 2-D tracks coated with gradients of adhesive proteins (24).

The ability of the cells to extend their protrusions across the channels may be attributed to the dynamics of actin polymerization and depolymerization. Using fluorescence speckle microscopy, Gupton *et al*. (20) showed that the lamellipodial protrusion was driven by the polymerization and depolymerization of actin located within 2-4 μm of the cell membrane's edge, commensurate with the length scale of our 2-μm channel width on the 2×2 and 5×2 patterns. This dynamic region of the lamellipodium

can propel a cell to successfully protrude across the channel and form a new adhesion site on the nearby ridge, thus enhancing cell migration transverse to the grooves.

Upon exposure to fluid shear stress, FAs and actin microfilaments in migrating endothelial cells undergo significant reorganization and remodeling (16, 27, 28). Within the time frame of our experiments, high, but not moderate levels of shear stress can effectively compete with microgrooves in guiding cell migration, possibly due to the dynamic reorganization of FAs (27). In our system, the cells respond to the high shear stress level of 58 dyn/cm$^2$ by extending their lamellipodia across the channels, allowing the formation of FAs in the flow direction. These newly formed FAs (see solid arrow, Fig. 7E) at the downstream side of the cells can initiate the coordinated migration steps (25, 27, 30, 35) transverse to the grooves, and may also induce the remaining FAs at the upstream side of the cells to gradually re-align with the flow, thus supporting cell migration in this transverse direction. We suspect that given sufficient time the cells on these orthogonally oriented microgrooves will eventually re-align their major axes with the flow. This notion is supported by previous studies (4, 33, 41) that have shown it generally takes around 24 h for endothelial cells on a smooth surface to adapt to flow under moderate shear stress (4, 41) and significantly longer at very low shear ($\leq$ 1 dyn/cm$^2$) (33).

The microgroove topography can create local shear stress gradients (9), similar to the distribution of shear stress over an endothelial monolayer (2, 4). The magnitude of shear stress reaches the maximum on the apical surface of the cells above their nuclei and is minimal near the basal surface (4). Analogous to the distribution of shear stress over the cell surface, numerical simulations of flow over a groove geometry (9) as well as a

spherical protuberance (32) predicted a significant reduction of shear stress inside the grooves and the near the base of the protuberance, respectively. For the groove geometry described by Daxini et al. (9), the fluid velocity and the wall shear stress acting parallel to the grooves decreased as a function of the groove depth. The average shear stress inside the 95-μm-wide channels was found to be about 28% less than that of a smooth surface, resulting in the retention of more cells inside the channels (9). Similarly, the numerical simulation of parabolic flow over a spherical cap also yielded a significant reduction in shear stress at the base level, compared to the top of the cap despite the formation of eddies at corners between the base level and the cap sidewall (32). In our study, the ridge-like protuberance (see Fig. 1) on the microgrooves oriented perpendicular to flow resembles this spherical cap geometry, with the channels formed at the base level. Based on these studies (4, 9, 32), we infer that the magnitude of shear stress inside the channels is lower than that at the ridges. This conclusion is supported by our observation of the cell protrusions preferentially extending down the channels (see top images, Fig. 4A).

The increase in directional cell migration and the cell retention under high shear stress can improve the endothelialization process in prosthetic vascular grafts. The groove-induced directional cell migration can promote the transanastomotic ingrowth of endothelial cells towards the midgraft, a process that remains absent in current graft models (42). In contrast to the non-unidirectional patterned surfaces, microgrooves alone mediate the unidirectional migration of endothelial cells and such directional cell migration is enhanced under the application of fluid shear stress acting parallel to the grooves. This guidance from microgrooves can facilitate the directional endothelial cell migration beyond the anastomotic region and further into the midgraft area. Unlike a

smooth surface, the topography of microgrooves can also provide additional anchorage sites for cellular attachment as demonstrated in the preferential alignment of FAs and actin microfilaments and the termination of cellular processes at the ridge edge (see Fig. 5F). In the presence of fluid shear stress, this groove-induced organization of FAs and actin microfilaments might strengthen cell anchoring on the substrate surface and retard the potential cell detachment with shear force. Even at the steady, shear stress of 58 dyn/cm$^2$, a level equivalent to the peak systolic shear stress in the abdominal aorta (5, 31), the endothelial cells in our study remain attached on the microgrooved substrate. This cell retention under high shear stress suggests that an endothelial monolayer grown inside a microgrooved vascular graft should be able to sustain the peak shear stress of the *in vivo* pulsatile arterial flow.

In summary, the width dimension of a 3-D microgroove topography plays an important role in guiding the direction of endothelial cell migration in the absence of flow as the groove width determines the spatial localization of FAs. The critical groove width at which the cells can significantly migrate across the microgrooves is found to be about 2 μm. Cues derived from shear stress on cell migration can be additive to or competitive with those derived from microgrooves, depending on the orientation of the grooves and flow, as well as the magnitude of shear stress. In terms of actin cytoskeleton, microgrooves, but not shear stress, guide the orientation of actin stress fibers parallel to the grooves after exposure to flow for at least 4 h. Local variation in shear stress over the microgroove topography may contribute to the preferential establishment of cellular protrusions inside the channels as the cells adapt to the area of reduced shear stress within the grooves. With all these considerations, the microgroove topography can facilitate

endothelialization of prosthetic grafts by increasing directional cell migration and strengthening cell retention under shear stress.

**ACKNOWLEDGEMENTS**

The authors acknowledge Mr. William Pennie and Mr. Michael Carman at the Instrumentation Shop (University of Pennsylvania) for the fabrication of the flow chamber, Dr. Gladys Lawrence (University of Pennsylvania) for her assistance on the confocal microscopy, Dr. Mark Lee (University of Pennsylvania) and Dr. Kenneth Barbee (Drexel University) for insightful discussion about cell migration, and Dr. A. T. Johnson for access to the e-beam lithography facility. We also thank Mr. Felice Macera (University of Pennsylvania) for the graphic assistance as well as Dr. Kevin Bittman and Mr. Mark Sobiesk (P3I) for their help with the real-time data acquisition and cell migration analysis.

**GRANTS**

This research was supported, in part, by grants-in-aid from the Nanotechnology Institute for the Southeastern Pennsylvania (to RJC and PIL), NASA (NAG2-1436, NNJ04HC81G-01, and NCC9-130 to PIL), NASA (NNCO5GA3OG), grants-in-aid from the Coulter Foundation (to PIL, RJC and RJL) and NSF (Polymers, DMR-05-49307 and Nano-Bio Interface Center, NSEC-04-25780 to RJC).

## REFERENCES


1. **Asahara T, Bauters C, Zheng LP, Takeshita S, Bunting S, Ferrara N, Symes JF and Isner JM**. Synergistic effect of vascular endothelial growth factor and basic fibroblast growth factor on angiogenesis in vivo. *Circulation* 92: 365-371, 1995.

2. **Barbee KA**. Role of subcellular-shear stress distributions in endothelial cell mechanotransduction. *Ann Biomed Eng* 30: 472-482, 2002.

3. **Barbee KA, Davies PF and Lal R**. Shear stress-induced reorganization of the surface topography of living endothelial cells imaged by atomic force microscopy. *Circ Res* 74: 163-171, 1994.

4. **Barbee KA, Mundel T, Lal R and Davies PF**. Subcellular distribution of shear stress at the surface of flow-aligned and nonaligned endothelial monolayers. *Am J Physiol* 37: H1765-H1772, 1995.

5. **Blackman BR, Garcia-Cardena G and Gimbrone MA**. A new in vitro model to evaluate differential responses of endothelial cells to simulated arterial shear stress waveforms. *J Biomech Eng-T ASME* 124: 397-407, 2002.

6. **Braddock M, Schwachtgen JL, Houston P, Dickson MC, Lee MJ and Campbell CJ**. Fluid shear stress modulation of gene expression in endothelial cells. *News Physiol Sci* 13: 241-246, 1998.

7. **Coan DE, Wechezak AR, Viggers RF and Sauvage LR**. Effect of shear stress upon localization of the golgi-apparatus and microtubule organizing center in isolated cultured endothelial-cells. *J Cell Sci* 104: 1145-1153, 1993.

8. **Davies PF**. Flow-Mediated Endothelial Mechanotransduction. *Physiol Rev* 75: 519-560, 1995.

9. **Daxini SC, Nichol JW, Sieminski AL, Smith G, Gooch KJ and Shastri VP**. Micropatterned polymer surfaces improve retention of endothelial cells exposed to flow-induced shear stress. *Biorheology* 43: 45-55, 2006.

10. **Dixit P, Hern-Anderson D, Ranieri J and Schmidt CE**. Vascular graft endothelialization: Comparative analysis of canine and human endothelial cell migration on natural biomaterials. *J Biomed Mat Res* 56: 545-555, 2001.

11. **Dolle JP, Rezvan A, Allen FD, Lazarovici P and Lelkes PI**. Nerve growth factor-induced migration of endothelial cells. *J Pharmacol Exp Ther* 315: 1220-1227, 2005.

12. **Dull RO and Davies PF**. Flow modulation of agonist (Atp)-response (Ca2+) coupling in vascular endothelial cells. *Am J Physiol* 261: H149-H154, 1991.

13. **Etienne-Manneville S and Hall A**. Rho GTPases in cell biology. *Nature* 420: 629-635, 2002.

14. **Folkman J**. Fundamental concepts of the angiogenic process. *Curr Mol Med* 3: 643-651, 2003.

15. **Frangos JA, McIntire LV and Eskin SG**. Shear stress induced stimulation of mammalian cell metabolism. *Biotech Bioeng* 32: 1053-1060, 1988.

16. **Girard PR and Nerem RM**. Shear stress modulates endothelial cell morphology and F-actin organization through the regulation of focal adhesion-associated proteins. *J Cell Physiol* 163: 179-193, 1995.

17. **Gojova A and Barakat AI**. Vascular endothelial wound closure under shear stress: role of membrane fluidity and flow-sensitive ion channels. *J App Physiol* 98: 2355-2362, 2005.

18. **Gotlieb AI, Subrahmanyan L and Kalnins VI**. Microtubule-organizing centers and cell migration: effect of inhibition of migration and microtubule disruption in endothelial cells. *J Cell Biol* 96: 1266-1272, 1983.

19. **Gottlieb AI, Langille BL, Wong MKK and Kim DW**. Structure and function of the endothelial cytoskeleton. *Lab Invest* 65: 123-137, 1991.

20. **Gupton SL, Anderson KL, Kole TP, Fischer RS, Ponti A, Hitchcock-DeGregori SE, Danuser G, Fowler VM, Wirtz D, Hanein D and Waterman-Storer CM**. Cell migration without a lamellipodium: translation of actin dynamics into cell movement mediated by tropomyosin. *J Cell Biol* 168: 619-631, 2005.

21. **Helmlinger G, Berk BC and Nerem RM**. Pulsatile and steady flow-induced calcium oscillations in single cultured endothelial cells. *J Vas Res* 33: 360-369, 1996.

22. **Herbst TJ, Mccarthy JB, Tsilibary EC and Furcht LT**. Differential effects of laminin, intact type-IV collagen, and specific domains of type-IV collagen on endothelial cell adhesion and migration. *J Cell Biol* 106: 1365-1373, 1988.

23. **Hsu PP, Li S, Li YS, Usami S, Ratcliffe A, Wang X and Chien S**. Effects of flow patterns on endothelial cell migration into a zone of mechanical denudation. *Biochem Biophys Res Commun* 285: 751-759, 2001.

24. **Hsu S, Thakar R, Liepmann D and Li S**. Effects of shear stress on endothelial cell haptotaxis on micropatterned surfaces. *Biochem Biophys Res Commun* 337: 401-409, 2005.

25. **Lauffenburger DA and Horwitz AF**. Cell migration: a physically integrated molecular process. *Cell* 84: 359-369, 1996.

26. **Li S, Kim M, Hu Y-L, Jalali S, Schlaepfer D, Hunter T, Chien S and Shyy JY-J**. Fluid shear stress activation of focal adhesion kinase. *J Biol Chem* 272: 30455-30462, 1997.

27. **Li S, Butler P, Wang Y, Hu Y, Han DC, Usami S, Guan JL and Chien S**. The role of the dynamics of focal adhesion kinase in the mechanotaxis of endothelial cells. *Proc Natl Acad Sci* 99: 3546-3551, 2002.

28. **Malek AM and Izumo S**. Mechanism of endothelial cell shape change and cytoskeletal remodeling in response to fluid shear stress. *J Cell Sci* 109: 713-726, 1996.

29. **Masuda M and Fujiwara K**. The biased lamellipodium development and microtubule organizing center position in vascular endothelial cells migrating under the influence of fluid flow. *Biol Cell* 77: 237-245, 1993.

30. **Mitchison TJ and Cramer LP**. Actin-based cell motility and cell locomotion. *Cell* 84: 371-379, 1996.

31. **Oshinski JN, Ku DN, Mukundan S, Loth F and Pettigrew RI**. Determination of wall shear stress in the aorta with the use of MR phase velocity mapping. *J Magn Reson Imaging* 5: 640-647, 1995.

32. **Pozrikidis C**. Effect of pressure gradient on viscous shear flow past an axisymmetric depression or protuberance on a plane wall. *Comput Fluids* 29: 617-637, 2000.

33. **Samet MM, Chick DM, Christensen CW and Lelkes PI**. Morphology and integrity of endothelial cell monolayers inside a ventricle shaped perfusion chamber. *ASAIO J* 39: M403-M409, 1993.

34. **Sato M, Kataoka N, Hashimoto K and Michihiro I**. Mechanical stress and actin filament dynamics in cultured endothelial cell. In: Tissue engineering for therapeutic use 4, edited by Ikada Y and Shimizu Y. Tokyo: Elsevier Science, 2000, p. 121-130.

35. **Shiu YT, Li S, Marganski WA, Usami S, Schwartz MA, Wang YL, Dembo M and Chien S**. Rho mediates the shear-enhancement of endothelial cell migration and traction force generation. *Biophys J* 86: 2558-2565, 2004.

36. **Truskey G and Pirone J**. The effect of fluid shear stress upon cell adhesion to fibronectin-treated surfaces. *J Biomed Mat Res* 24: 1333-1353, 1990.

37. **Tsuruta D and Jones JCR**. The vimentin cytoskeleton regulates focal contact size and adhesion of endothelial cells subjected to shear stress. *J Cell Sci* 116: 4977-4984, 2003.

38. **Urbich C, Dernbach E, Reissner A, Vasa M, Zeiher AM and Dimmeler S**. Shear stress-induced endothelial cell migration involves integrin signaling via the fibronectin receptor subunits alpha(5) and beta(1). *Arterioscler Thromb Vasc Biol* 22: 69-75, 2002.

39. **Uttayarat P**. *Chemical and physical modifications of silicone for novel vascular grafts* (Dissertation). Department of Materials Science and Engineering, University of Pennsylvania, 2007.

40. **Uttayarat P, Toworfe GK, Dietrich F, Lelkes PI and Composto RJ**. Topographic guidance of endothelial cells on silicone surfaces with micro- to nanogrooves: orientation of actin filaments and focal adhesions. *J Biom Mat Res A* 75: 668-680, 2005.

41. **Wojciak-Stothard B and Ridley AJ**. Shear stress-induced endothelial cell polarization is mediated by Rho and Rac but not Cdc42 or PI 3-kinases. *J Cell Biol* 161: 429-439, 2003.

42. **Zilla P, Bezuidenhout D and Human P**. Prosthetic vascular grafts: Wrong models, wrong questions and no healing. *Biomaterials* In Press, Corrected Proof.

**Figure legends**

**Fig. 1.** Schematic of a combinatorial array (A) and SEM images (B to E) of four microgroove patterns on PDMS substrate. *A*: each pattern is repeated four times down the same column and twice within the same row, yielding a total of 32 patterned areas. Lines represent the horizontal and vertical directions of grooves. Cross-sectional profiles of the four microgrooves, 5×5 (B), 3×3 (C), 2×2 (D), and 5×2 (E) are visualized by SEM. Scale bars are 10 μm.

**Fig. 2.** Bar graph of endothelial cell alignment after 1 h of cell attachment. Data are means ± SE from 3 independent experiments with a total of about 200 cells. Above the angle of orientation 0-5 and 10-15 (see measurement in MATERIALS AND METHODS), dashed lines represent the cells' major axes and solid lines represent the groove direction.

**Fig. 3.** Endothelial cell migration in the absence of flow. Data are means ± SE from 7 independent experiments. *A*: cells are grouped according to their migration directions during 4 h time-lapse observation. $^{*}P \leq 0.05$ vs. transverse direction on 5×5, 3×3 and 2×2 patterns. *B*: migration velocities of the cells in (A) are calculated from the traced total distance over 4 h. $^{*}P \leq 0.05$ vs. transverse direction on 3×3 and 2×2 patterns.

**Fig. 4.** Endothelial cell migration on microgrooves under flow. Data are means ± SE for cell migration in the direction of flow during 4 h time-lapse observation from 5

independent experiments. *A*: microgrooves oriented parallel to flow. *B*: microgrooves oriented perpendicular to flow. For comparison, white solid bars represent data from static conditions (see Fig. 3). Moderate and high shear correspond to shear stress levels of 13.5 and 58 dyn/cm$^2$, respectively. $^{*}P < 0.05$ vs. static. $^{\#}P < 0.05$ vs. moderate shear. $^{+}P < 0.05$ vs. static. *Top*: selected images of cells (pseudo-colored in red) overlayed on microgrooves. Dashed lines guide the direction of grooves. Channels appear in light contrast. *A, top*: cells migrating parallel to grooves on 3×3 pattern showing a cell (solid arrows) enters a microgrooved area at t = 0 and filopodial extension along the channel (arrow heads). *B, top* cell migrating transverse to grooves on 5×5 pattern showing a single protrusion (solid arrows) and protrusions from both cell ends (arrow heads). Scale bars are 50 μm for all images.

**Fig. 5.** Organization of actin microfilaments under static (A-C) and high shear (D-F) conditions. Cells were fixed after 4 h migration experiments and stained with TRITC-conjugated phalloidin for actin microfilaments (shown in red). *A, D*: smooth surfaces, *B, E, F*: 5×5 patterns and *C*: 5×2 pattern. The letters **C** and **R** refer to channels and ridges, respectively. Dashed lines represent microgrooves underneath cells. Solid arrows and arrow heads are explained in text (see RESULTS). *D, E, F*: Flow arrows indicate the direction of flow. Scale bars in (A) and (D) are 50 μm and applied to all images taken under static and high shear conditions, respectively.

**Fig. 6.** Confocal images of immunostained vinculin (green) associated with focal adhesions (FAs) in the absence of flow on smooth (A) and microgrooved (B, C) surfaces.

For FA distribution analysis, confocal images are overlayed on micrgrooves as shown on the 5×5 (B) and 5×2 (C) patterns. Arrows are explained in text (see RESULTS). The letters **C** and **R** refer to channels and ridges, respectively. Dashed lines guide the direction of grooves. *B,C*: channels are in light contrast. Scale bars are 5 μm.

**Fig. 7.** Organization of focal adhesions (FAs) under flow on smooth (A and B) and microgrooved (C, D and E) surfaces visualized by confocal microscopy. After 4 h of cell migration under flow, cells were fixed and immunostained for vinculin (green) associated with FAs. As illustrated in (A), flow direction is indicated by flow arrow and applied to all images. *C,D,E*: confocal images are overlayed on microgrooves with channels appear in light contrast. *C:* 3×3 pattern. *D, E*: 5×2 patterns. Arrows are explained in text (see RESULTS). Dashed lines guide the direction of grooves. Scale bars are 5 μm.

**Table 1.** The dimensions of microgrooves on PDMS

| Patterns | Ridge (μm) | Channel (μm) |
|---|---|---|
| 5×5 | 5.04 (± 0.07) | 4.84 (± 0.07) |
| 3×3 | 2.86 (± 0.03) | 2.97 (±0.04) |
| 2×2 | 2.12 (± 0.03) | 1.73 (± 0.03) |
| 5×2 | 5.00 (± 0.05) | 1.69 (± 0.04) |

The ridge and channel widths are measured at a height that is at the half maximum between the ridge and channel. Values are means ± SE.

**Table 2.** Shape factor of endothelial cells on smooth and microgrooved surfaces

| Surfaces | Static | High Shear Stress | |
|---|---|---|---|
| | | parallel to grooves | perpendicular to grooves |
| smooth | 0.40 (± 0.04) | 0.48 (± 0.03) | |
| 5×5 | 0.35 (± 0.03) | 0.46 (± 0.03) | 0.47 (± 0.03)* |
| 3×3 | 0.36 (± 0.03) | 0.37 (± 0.02) | 0.51 (± 0.03)*,+ |
| 2×2 | 0.35 (± 0.03) | 0.44 (± 0.05) | 0.51 (± 0.03)* |
| 4×2 | 0.39 (± 0.02) | 0.45 (± 0.04) | 0.53 (± 0.03)* |

Data were collected for static and high shear conditions from 3 independent experiments with a total of about 80 to 110 cells. Values are means ± SE. $^{*}P < 0.05$ vs. static. $^{+}P < 0.05$ vs. parallel.

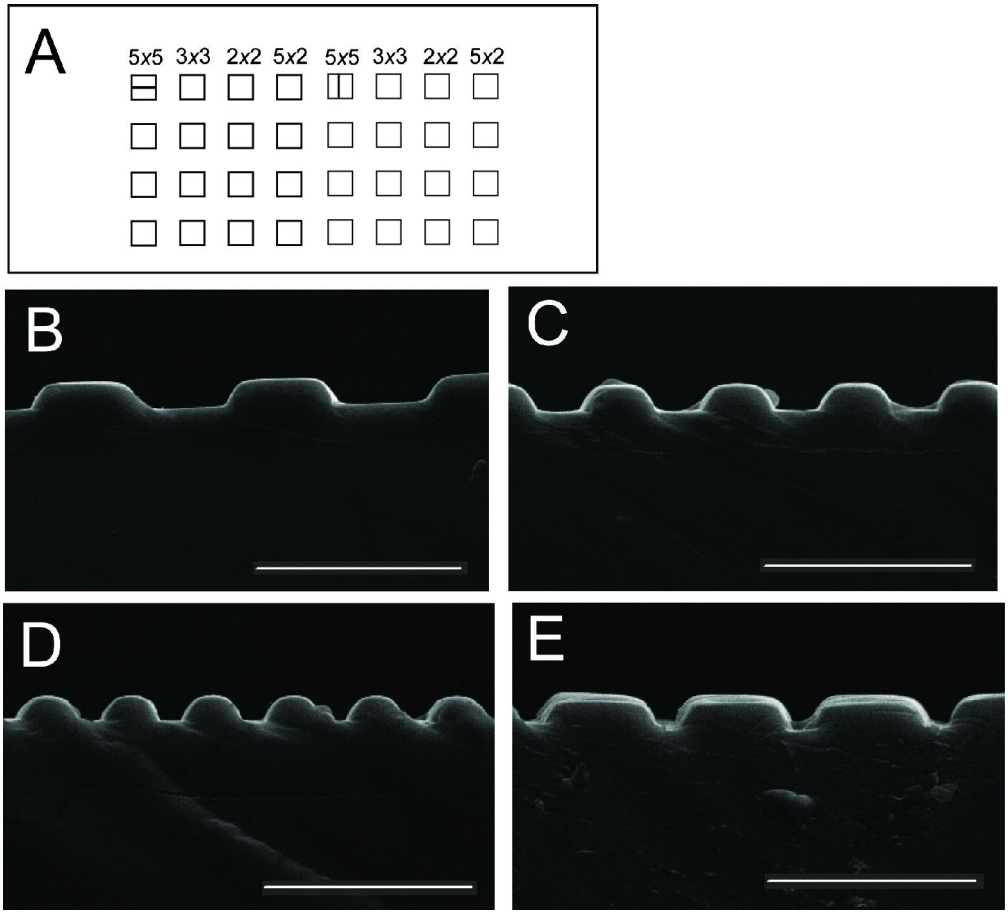


**Fig. 1**
80x72mm (600 x 600 DPI)

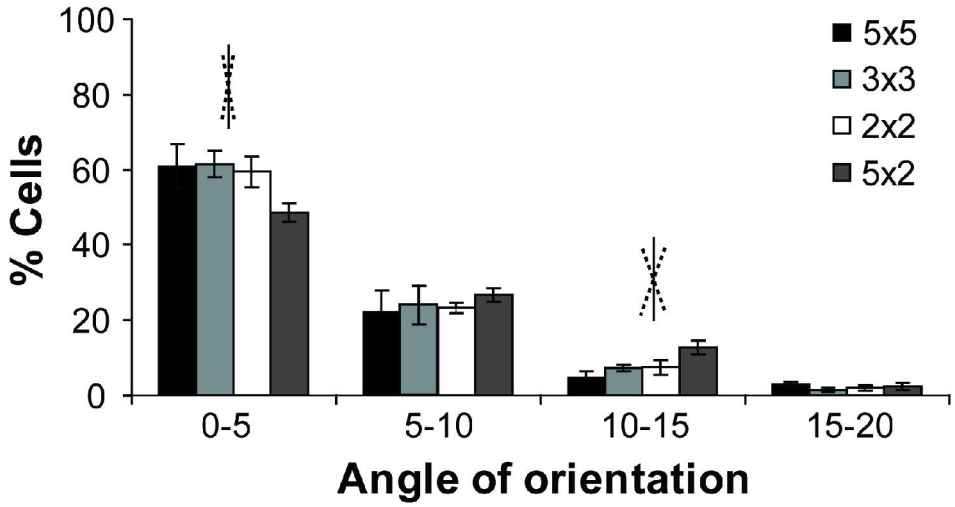


**Fig. 2**
81x51mm (600 x 600 DPI)

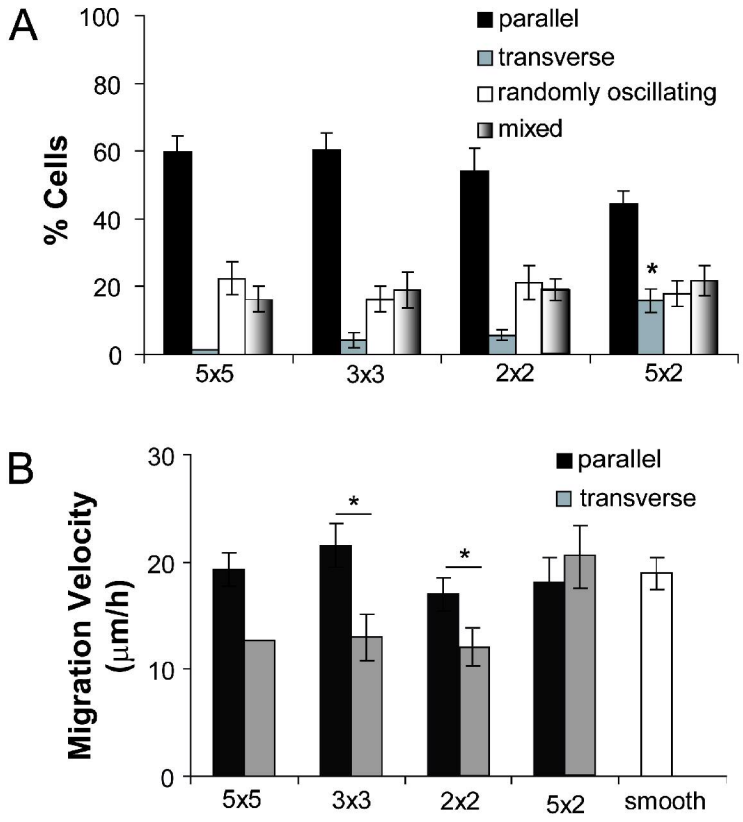


**Fig. 3**
97x135mm (600 x 600 DPI)

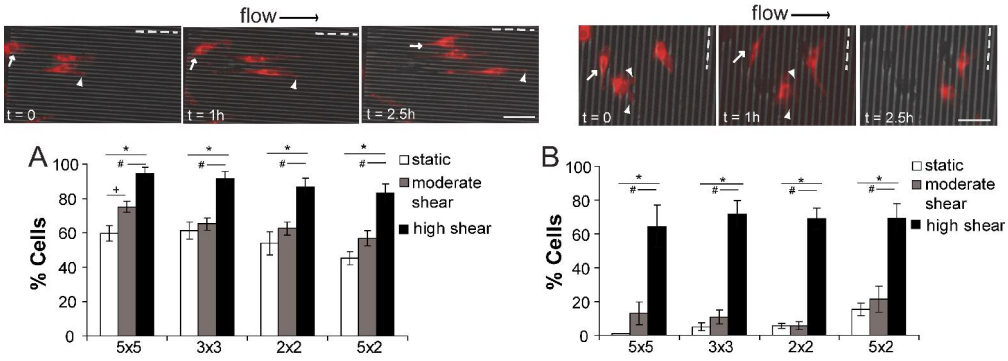


**Fig. 4**
170x61mm (600 x 600 DPI)

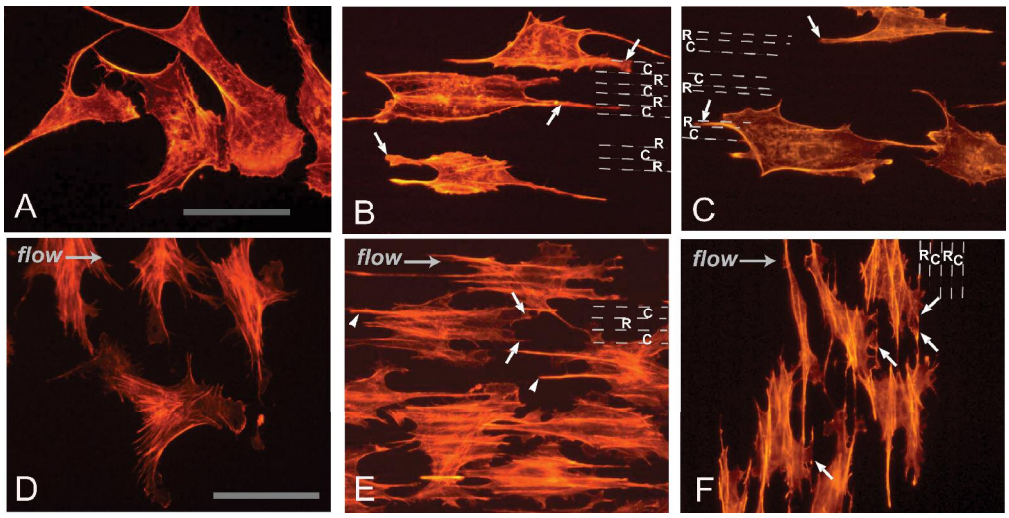


**Fig. 5**
125x63mm (600 x 600 DPI)

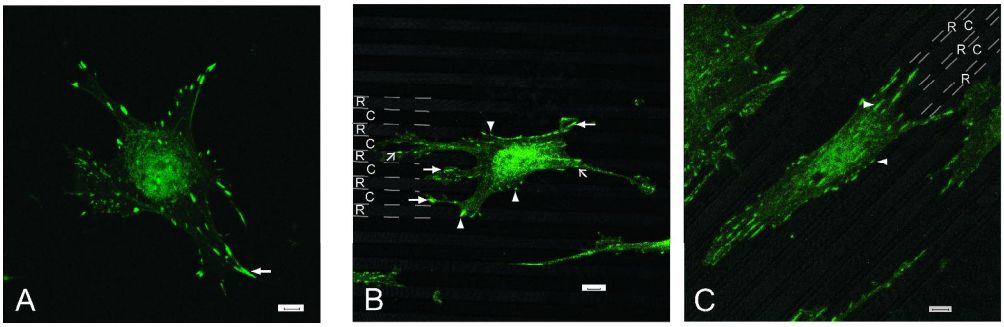


**Fig. 6**
136x43mm (600 x 600 DPI)

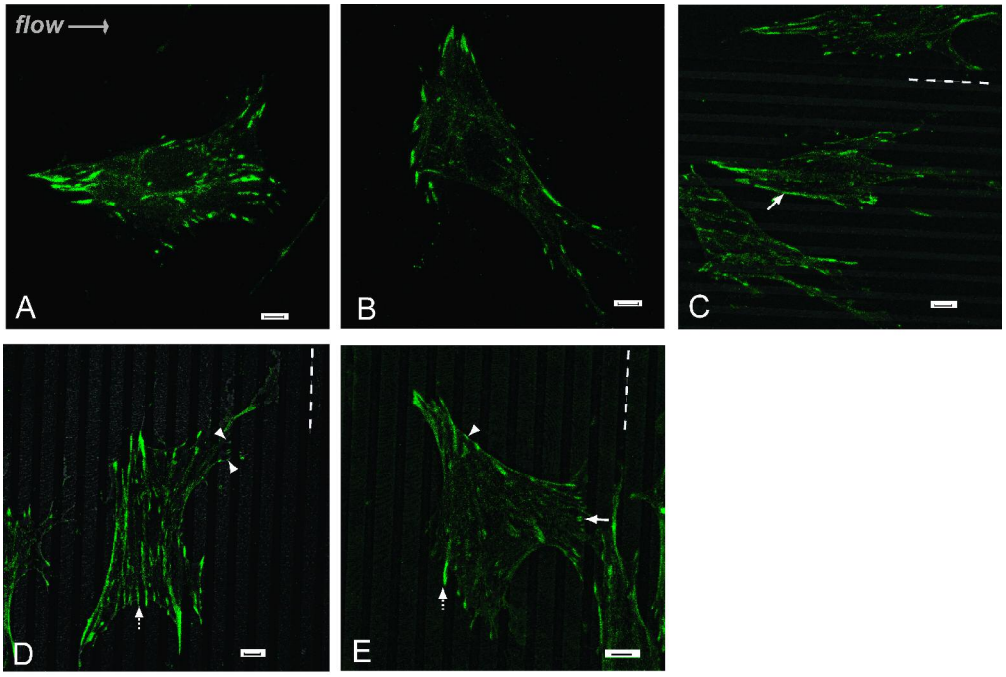


**Fig. 7**
159x106mm (600 x 600 DPI)